



Contents lists available at ScienceDirect

Deep-Sea Research I

journal homepage: www.elsevier.com/locate/dsri

On the warm/cold regime shift in the South China Sea: Observation and modeling study

P. Swapna^a, Jianping Gan^{a,b,*}, Alexis Lau^c, Jimmy Fung^b

^a Atmospheric, Marine, Coastal Environment (AMCE) Program, Hong Kong University of Science and Technology, Clear Water Bay, Kowloon, Hong Kong

^b Department of Mathematics, Hong Kong University of Science and Technology, Clear Water Bay, Kowloon, Hong Kong

^c Department of Civil Engineering, Hong Kong University of Science and Technology, Clear Water Bay, Kowloon, Hong Kong

ARTICLE INFO

Article history:

Received 29 May 2008
Received in revised form
13 March 2009
Accepted 23 March 2009
Available online 5 April 2009

Keywords:

Sea level anomaly
Heat transport
Climate variability

ABSTRACT

Remote sensing data sets and a high-resolution three-dimensional regional ocean model were utilized to investigate the shifting of warm/cold regime and the associated sea level variation in the South China Sea (SCS) during 2000–2003. Both the altimetry data and the model results showed an increase in the sea level (warm phase) followed by an abrupt decrease (cold phase) in the SCS during 2000–2003. Heat budget calculations performed with the model revealed excess heat advection from the western Pacific warm pool into the SCS during the warm phase than the cold phase. The warm phase, which occurred during La Niña episodes, resulted from the intrusion of abnormally warmer western Pacific water that increased the heat content and thus sea level in the SCS. The cold phase, which occurred during El Niño episodes, was triggered by a reduction in the net atmospheric heat flux followed by cold water advection into the SCS. Decrease in the rate of precipitation minus evaporation ($P-E$) also accounted for the falling of sea level during cold phase. The present study integrated the available remote sensing data and advanced numerical model to identify the time-dependent three-dimensional dynamic and thermodynamic forcing that are important in governing the warm/cold regime shift in the SCS.

© 2009 Elsevier Ltd. All rights reserved.

1. Introduction

Global warming is emerging as one of the key issues having ramifications on regional climate variability. Recently, the Intergovernmental Panel on Climate Change published its 4th assessment report (IPCC, AR4, 2007) addressing climate change due to global warming. One of the catastrophic consequences of global warming is the rise in sea level. Global sea level rose at an average rate of about 1.8 mm year^{-1} from 1961 to 2003 and sea level rise was 3.1 mm year^{-1} from 1993 to 2003 (Cazenave and Nerem, 2004; Holgate and Woodworth, 2004).

Though the issue of global sea level rise has received considerable attention in the last decade (e.g., Gregory et al., 2001; Antonov et al., 2002, 2005; Munk, 2002; Cazenave and Nerem, 2004; Carton et al., 2005; Landerer et al., 2006), there are still uncertainties in understanding the physical processes leading to regional sea level variations. Sea level change is found to be highly non-uniform spatially, with certain regions undergoing rising rates up to several times that of the global mean rise, while in other regions sea level is falling (IPCC, AR4). In the South China Sea (SCS), few studies have addressed the inter-annual variations in sea level. Earlier studies focused on the seasonal variations in sea level in the SCS. Using Topex/Poseidon data for a short period, Shaw et al. (1999) and Ho et al. (2000) showed that sea level in the SCS is higher west of the Luzon Strait and the Taiwan Strait during summer and is lower during winter. This seasonal

* Corresponding author at: Atmospheric, Marine, Coastal Environment (AMCE) Program, Hong Kong University of Science and Technology, Clear Water Bay, Kowloon, Hong Kong.

E-mail address: magan@ust.hk (J. Gan).

variability was attributed to seasonally reversing monsoon winds.

With the availability of satellite data, long time series of sea level data are available for studying inter-annual trends. Using Topex/Poseidon data, Li et al. (2002) found that the mean sea level in the SCS rose at a rate of $10.0 \text{ mm year}^{-1}$ from 1993 to 1999 with higher values located west of the Luzon Strait. The geographical distribution of sea level was found to be non-uniform in the SCS. Cheng and Qi (2007) used a longer time series of merged altimetry data from 1993 to 2006 and showed a sea level rise of about $11.3 \text{ mm year}^{-1}$ in the SCS during 1993–2001, which is much larger than the global average of 3.1 mm year^{-1} derived from satellite estimates. Interestingly, the study also revealed a decrease in sea level in the SCS during 2001–2005. The study by Fang et al. (2006), using sea surface height from satellite altimetry data, also reported a long-term positive trend in sea level from 1993 to 2001 and a reversal in the sign of this trend from 2001 to 2003. However, the process and mechanism contributing to these dramatic shifts in sea level, which are essential for understanding the warm/cold regime in the SCS, have not been established.

Sea level variation in the SCS from merged altimeter data from 1993 to 2006 is presented in Fig. 1a. The detailed description about the data is presented in Section 2. The time series in Fig. 1a shows a sea level increase in the SCS during 1993–2000 and a sea level fall during 2001–2005. The variations in the sea level were closely associated with the occurrence of El Niño/La Niña in the Pacific. The time series of Niño 3.4 SST index is

shown in Fig. 1b. Based on the definition of Trenberth (1997), if a 5-month running mean of sea surface temperature (SST) anomalies in the Niño 3.4 region (5°N – 5°S , 120°W – 70°W) exceeds 0.4°C for 6 months or more, then the year is defined as an El Niño year. It can be seen from the figure that the La Niña events are generally followed by an increase of sea level in the SCS, while sea level falls during El Niño periods. The sea level in the SCS showed an increase from January 1998 till December 2000 in association with the La Niña period and the sea level decreased slowly during the transition period from La Niña to El Niño episode. Then the sea level fell rapidly during 2001–2005 in association with the subsequent El Niño period.

The dynamic and thermodynamic forcing processes that caused this observed sea level rise and fall in the SCS are, however, not yet understood. This “enigma” is caused by the uncertainty of circulation induced by complex topography of the SCS (Fig. 2) which leads to uncertainty in the heat budget calculation. This includes the mass and heat transports through the narrow straits (e.g., Taiwan Strait, Luzon Strait, and Karimata Strait) that connect the SCS with the surrounding seas and the Pacific Ocean. The SCS connects to the Pacific through the Luzon Strait in the north and to the Java and Sulu Seas to the south through a number of shallow passages. The circulation in the SCS is influenced by El Niño and La Niña in the Pacific (Xie et al., 2003; Wang and Wang, 2006; Wang et al., 2006). The weakening (strengthening) of the northeasterly winds during winter and the strengthening (weakening) of the southwesterly winds during summer, associated with El

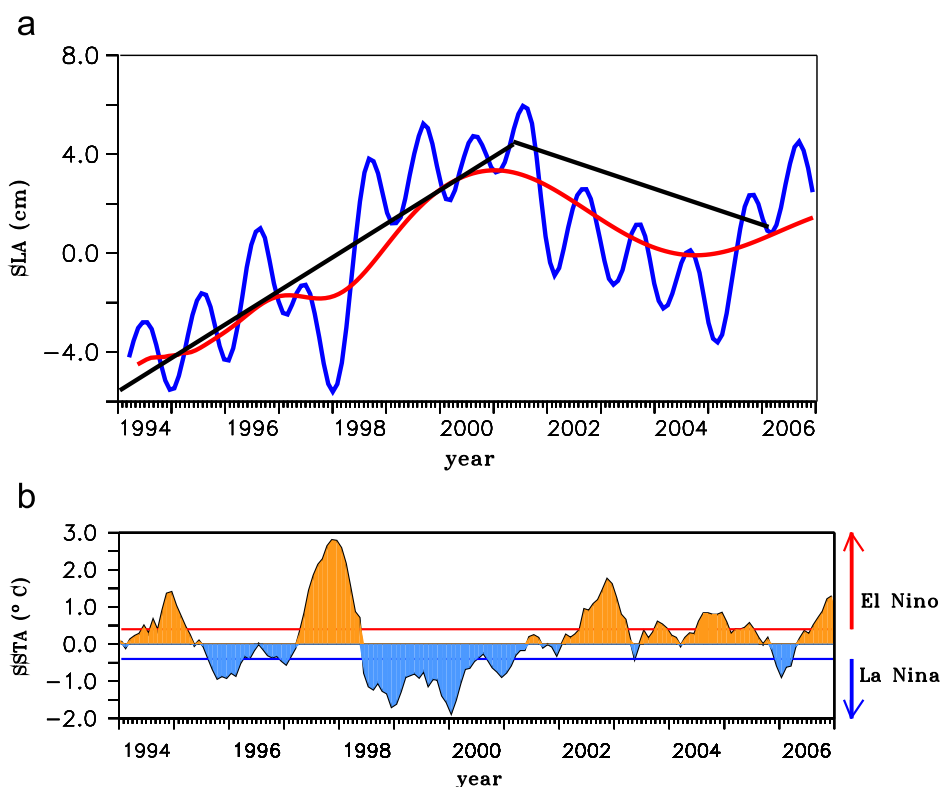


Fig. 1. (a) Time evolution of sea level anomalies (cm) from the altimeter data for the South China Sea domain. The red curve shows the anomalies after removal of the semi-annual cycle. (b) Time series showing the Niño 3.4 (5°N – 5°S , 120° – 70°W) SST index (for interpretation of the references to colour in this figure legend, the reader is referred to the web version of this article).

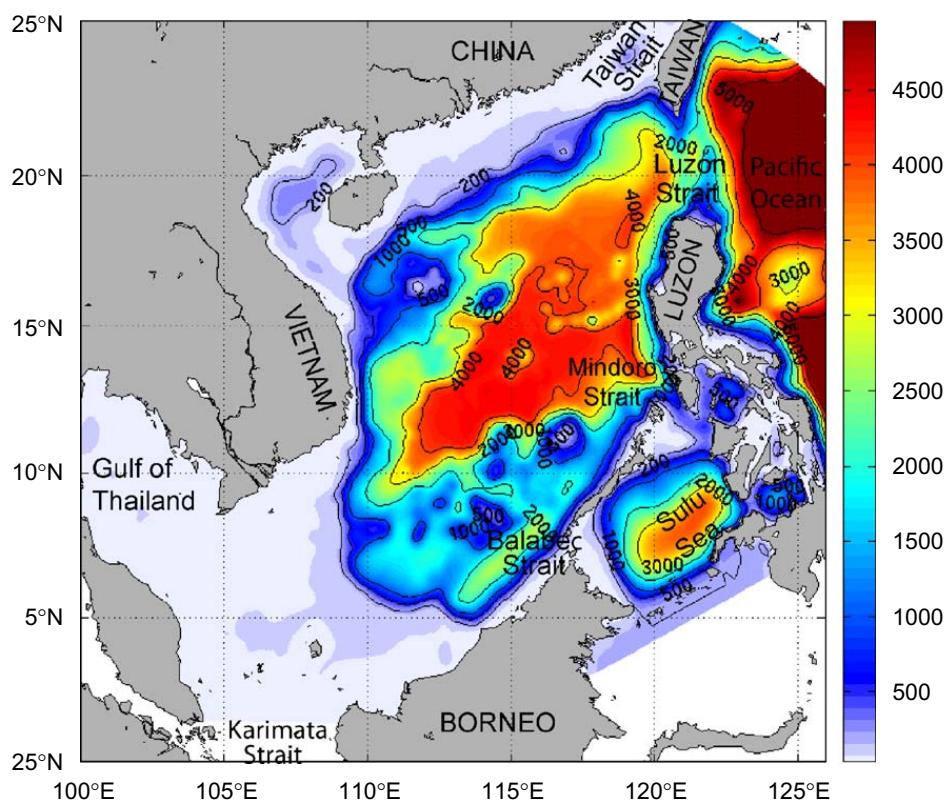


Fig. 2. Bathymetry of the model domain.

Niño (La Niña) induce upper layer circulation changes in the SCS. The modeling study on the inter-annual variability of circulation in the SCS by Wang et al. (2006) showed weakening of cyclonic circulation during the winter of 1997 associated with El Niño and the formation of an anomalous anticyclonic gyre during the summer of 1998 associated with La Niña. The ENSO also affects the heat budget of the SCS. The warm and saline water from the Kuroshio of the Pacific enters the SCS through the Luzon Strait and induces the strong influence of ENSO in the SCS (Qu et al., 2004). Accordingly, Luzon Strait transport exhibits inter-annual variation associated with ENSO. The study by Qu et al. (2004) found that Luzon Strait transport is stronger during El Niño years and is weaker during La Niña years.

The thermal change in the upper layers of the water column was found to be the prime mechanism for the sea level variation in the SCS in the study by Cheng and Qi (2007). They found that, during El Niño years, more water from the Pacific penetrates into the SCS through the Luzon Strait and water with higher temperature leaves the SCS through the passages in the south, cooling the SCS and lowering the sea level. However, the study by Zheng et al. (2007) reported a greater intrusion by the Kuroshio during La Niña years than the El Niño years. The study by Rong et al. (2007) showed that the volume transport between the SCS and the adjacent oceans and anomalous Ekman pumping contribute to the sea level fall during the developing stage of El Niño.

Though the above studies discussed the sea level variability in the SCS during the same period, they described different mechanisms for the sea level rise

and fall during 1993–2005. This may be due to the lack of high-resolution data to better depict the mass and heat transports through the narrow passages connecting the SCS to the adjacent seas and the Pacific Ocean. In the present study, we have used a three-dimensional high-resolution (~10 km, 30 vertical sigma level) regional model of the SCS (Gan et al., 2006) to investigate the enigma in sea level variation in the SCS during 2000–2003.

2. The ocean model and data used for the study

2.1. Ocean model

The high-resolution ocean model used for this study is the Princeton Ocean Model (POM), for three-dimensional, time-dependent oceanographic flows governed by hydrostatic primitive equations (Blumberg and Mellor, 1987). The Mellor and Yamada (1982) level 2.5 turbulent closure scheme was used to parameterize the vertical mixing. The model domain extends from 1.5°N to about 26°N in the north–south direction and from about 100°E to 130°E in the east–west direction. It included the region east of the Philippines so that Kuroshio dynamics could be incorporated. A curvilinear horizontal grid was utilized with 259×181 grid points in the horizontal and 30 levels in the vertical. The horizontal grid spacing was variable, with small spacing (nearly 10 km) in the northern and central parts of the domain and larger grid spacing (nearly 20–30 km) in the eastern and southern parts of the domain. Active open boundary conditions, developed by

Gan and Allen (2005b) and successfully applied in a limited-area modeling study (Gan et al., 2005), were implemented at the eastern and southern open boundaries. More details about the model can be obtained from Gan et al. (2006).

The model was initialized with the 7-year mean winter (1997–2003; December–February) temperature and salinity from the regional ocean modeling system for the Pacific (Curchitser et al., 2005). The Pacific model domain covers the region from 30°S to 65°N and 100°E to 70°W with a horizontal grid size of 40 km and 30 vertical levels. The forcing for the hindcast stage of the simulation in the Pacific Ocean model was derived from the daily NCEP data set. After an initial spin-up of 10 years, the Pacific Ocean model was run in hindcast mode for years 1997–2003 and outputs of every 3-day average are archived to provide the lateral fluxes for the SCS model.

The SCS model was spun up for 1500 days. The spin-up was forced with the 7-year mean wind stress in the winter, derived from $1^\circ \times 1^\circ$, 6 hourly NCEP data and with the 7-year mean winter lateral fluxes at the open boundaries. The 7-year mean heat flux was also applied during the spin-up period. Then the inter-annual simulations were performed with time-dependent atmospheric and lateral fluxes from 1 January 2000 to 30 June 2003. The model was found to be successful in reproducing the mean circulation in the SCS (Gan et al., 2006).

The data from the ocean reanalysis product, simple ocean data assimilation (SODA; Carton et al., 2000) were also used for the study. The ocean model component is based on the Parallel Ocean Program 1.3 numerical representation of the Boussinesq primitive equations. This ocean model has 900×601 grid points with an average $0.25^\circ \times 0.4^\circ$ resolution. The vertical resolution is 10 m near the surface with a total of 40 vertical levels. Vertical diffusion is based on the KPP parameterization of Large et al. (1994), while horizontal diffusion is biharmonic. Topography is based on the ETOPO30 data of Smith and Sandwell (1997) with a few modifications to ensure reasonable basin exchange rates. A sequential assimilation algorithm is used to assimilate the observations and the reanalysis product has a resolution of $0.5^\circ \times 0.5^\circ$ with 40 levels in the vertical. The results from SODA were compared with POM results and were also used for the analysis of western Pacific region.

2.2. Data

The sea level variations in the SCS were studied using merged altimetry data. Sea level anomaly (SLA) data from merged Topex/Poseidon, Jason and ER-1/2, or Envisat SLA data distributed by CLS Space Oceanography Division was also used for the study (see <http://www.avisioceanobs.com/html>). Weekly data from January 1994 to December 2006 was used to prepare the monthly sea level anomalies. The long-term mean was removed and a 3-month moving average was applied to get the time series. Though the satellite altimetry gives valuable information on the global sea level, its results in shelf regions are still to be improved due to inaccurate

de-tiding (Bosch et al., 2006). Hence, we have used altimetry data in the deeper regions, covering water depths more than 200 m, for the study. For consistency, all the other data sets used to prepare the time series were also averaged for water depth greater than 200 m in the SCS.

The atmospheric parameters employed in the data diagnostic included the atmospheric heat fluxes from the National Centre for Environmental Prediction (NCEP; Kistler et al., 2001) and the precipitation data from Climate Prediction Center Merged Analysis of Precipitation (CMAP; Xie and Arkin, 1997). Both data sets have a resolution of $2.5^\circ \times 2.5^\circ$. The sea surface temperature was from $1^\circ \times 1^\circ$ resolution OISST derived from an optimal interpolation technique that regressed satellite retrievals against *in situ* ship and buoy observations (Reynolds optimum interpolated SST; Reynolds and Smith, 1994). These data sets were for the period 1994–2006. The high-resolution SST data were required for comparing the high-resolution model results. We have used 4 km resolution SST from the Moderate Resolution Imaging Spectroradiometer (MODIS) for the period 2000–2003.

3. Factors affecting sea level variation

The changes in the sea level represent a combination of changes that include changes of the mass of the oceans due to water-mass exchange, melting of continental ice, and filling of continental reservoirs (*eustatic changes*); changes in the thermal and haline structure of the oceans (*steric changes*); and geologic changes that cause vertical crustal movements of tide gauges, mainly from post-glacial rebound (Church et al., 2001; Carton et al., 2005). However, for a tropical sea like SCS, the water-mass exchange and the steric changes can be considered as the prime mechanism causing sea level variations. Levitus et al. (2005) pointed out that, during the last decade, the temperature of the global oceans has increased by 0.037°C in the upper 3000 m and that this thermal expansion of the ocean contributes significantly to global sea level rise. However, the studies by Willis et al. (2004) and Antonov et al. (2005) showed that thermosteric (temperature) sea level rise for the global oceans accounts for only half the sea level variation detected by satellite estimates and the input of fresh water into the oceans explains the remainder of sea level rise (Antonov et al., 2002). The study by Ishii et al. (2006) showed that sea level variations are caused mainly by temperature changes and that the effect of salinity variations is significant at higher latitudes and in the Atlantic Ocean. This is also supported by the study of Kang et al. (2005) who analyzed the sea level variations in the East/Japan Sea (EJS) using altimetry and tide gauge data and found that the sea level rise in the EJS is mainly due to thermal expansion.

Thermosteric and halosteric (salinity) sea level variations can be represented by steric sea level changes. The steric sea level change represents the vertical expansion or contraction of the water column in response to changes in the local density structure caused by thermosteric and halosteric variations. According to Landerer et al. (2006),

sea level variation can be represented as follows:

$$\eta' = \eta'_a + P'_b g^{-1} \rho_0^{-1} + \eta'_s \quad (1)$$

where prime represents variations with respect to time, η'_a the barometric correction to sea level, $P'_b g^{-1} \rho_0^{-1}$ the contribution from bottom pressure changes, and η'_s the steric sea level variation. The barometric correction to sea level is assumed to be zero.

The steric sea level deviation η'_s is given by

$$\eta'_s = \int_{-H}^0 \frac{\rho_0(x,y,z) - \rho(x,y,z,t)}{\rho_0(x,y,z)} dz \quad (2)$$

or

$$\eta'_s = - \int_{-H}^0 \frac{\rho'}{\rho_0} dz \quad (3)$$

η'_s represents the change in the volume of the ocean without changing the mass of the ocean. Any changes in the temperature and salinity of the water column can cause the thermal expansion/contraction of the water column by changing the heat content and steric variation in sea level. Thus, Eq. (1) implies that the total sea surface height and steric height are only equivalent if bottom pressure changes are zero. The difference between the total sea level change η' and steric sea level variation η'_s gives the bottom pressure change which is equivalent to the mass redistribution within the oceans. Thus, the total sea level variation can be represented as the sum of the steric sea level deviation and mass redistribution. In the SCS, the mass redistribution can be considered as South China Sea throughflow, which involves the inflow through the Luzon Strait and the outflow through the Karimata, Mindoro, and Taiwan Straits (Qu et al., 2005, 2006).

4. Results and discussion

To understand the sea level variation in the SCS, each of those factors that affect the temperature and salinity variations in the SCS and the mass and heat exchange between the SCS and the adjacent seas and the Pacific was examined. Thermal expansion of the water column is caused by net heating at the surface of the ocean or the entire water column. In addition to this, El Niño/La Niña in

the Pacific influences the sea level variations in the SCS to a larger extent by changing the dynamic condition, and, hence, the mass and heat transport cross the Luzon Strait. In the following analysis we examine the factors that affect the sea level at the ocean surface and the entire water column including the water and heat exchange between the SCS and the Pacific Ocean.

4.1. Net atmospheric heat flux

The exchange of heat and fresh water (evaporation/precipitation) between the ocean and the atmosphere modifies the density of the ocean and, hence, the sea level of the ocean. In an extensive review, Cazenave and Nerem (2004) pointed out that the recent increase in sea level in global oceans may be due to an increase in heat storage within the ocean and that such an increase only required a net global increase in surface heat flux of $1\text{--}2 \text{ W m}^{-2}$ (Willis et al., 2004).

The net atmospheric heat flux anomalies were computed from the NCEP data for the SCS domain:

$$Q_{net} = LHF + SHF + LW + SW \quad (4)$$

where LHF is the latent heat flux (W m^{-2}), SHF the sensible heat flux (W m^{-2}), LW the long wave radiation flux (W m^{-2}), and SW the shortwave radiation flux (W m^{-2}) at the surface of the ocean. The positive values of heat flux represent the ocean gaining heat from the atmosphere.

The net atmospheric heat flux anomalies, averaged for the SCS domain, for water depth greater than 200 m are presented in Fig. 3 (black solid line). The net-heat flux reached maximum positive values during January 1997 and was associated with the strongest El Niño of the last century. During the El Niño years, there was a reversal in the atmospheric Walker circulation with anomalous ascent over the central and eastern part of the equatorial Pacific and anomalous descent over the equatorial Indo-western Pacific region (Klein et al., 1999). The proximity of the SCS to the anomalous descent region induced reduction in wind speed and cloudiness over the SCS. Shortwave radiation increased and latent heat loss from the ocean decreased. A combination of these caused an anomalous

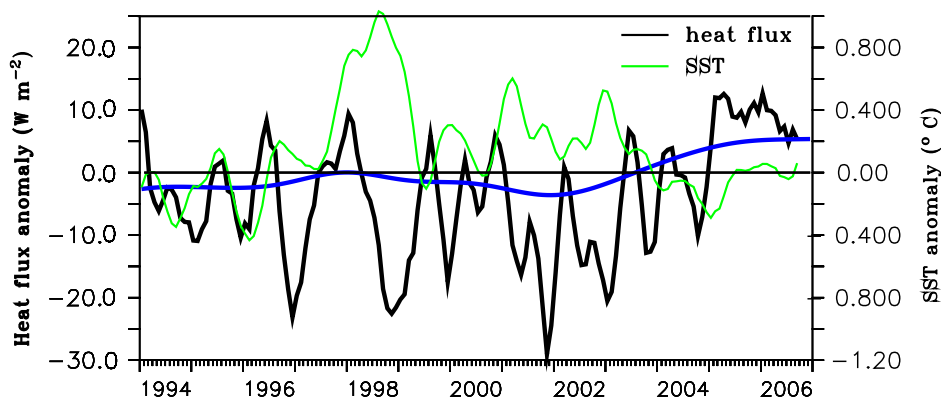


Fig. 3. Time evolution of SST anomalies ($^{\circ}\text{C}$) and net-heat flux anomalies (W m^{-2}) for the South China Sea domain. The blue curve represents the net-heat flux anomalies after removal of the semi-annual cycle (for interpretation of the references to colour in this figure legend, the reader is referred to the web version of this article).

increase in the net heating to the SCS during and after the mature phase of El Niño.

When the heat flux reached maximum value during January 1997, the sea level was the lowest in the SCS (Figs. 3 and 1). Then the negative anomalies of net-heat flux increased during La Niña and reached a minimum value in December 2001. The sea level anomalies increased during this period and the net-heat flux variation was found to be out of phase with the seasonal variation of the sea level anomalies. However, during December 2001, when the La Niña phase changed into El Niño, the heat flux reached minimum and the sea level fell dramatically in the SCS. The La Niña phase decayed by March 2001 and the El Niño started to develop by March 2002. During this transition period, the heat flux and the sea level variations were found to be correlated well in the SCS domain. The minimum in the heat flux during December 2001 coincided with the beginning of decreasing phase in sea level in the SCS. Again atmospheric heating to the SCS increased with El Niño, but the sea level continued to fall in the SCS until December 2004 before a new regime started.

The sea surface temperature anomalies (green curve in Fig. 3) also show inter-annual variations similar to the heat flux anomalies. During most of the period of study, the SST anomalies were positive except between 1994 and 1996 and after 2003. The SST anomalies were negatively correlated with the net atmosphere heat flux anomalies except during 1994–1996, and were generally not correlated with the sea level variations. Wang et al. (2006) showed that the SST in the SCS is largely influenced by ENSO. The SCS SST anomalies lagged the Niño 3 SST by 5 months (Klein et al., 1999; Wang et al., 2000).

4.2. Precipitation minus evaporation

Freshwater exchange via salinity variation has a secondary effect on sea level variability. However, salinity effects were found to be significant over certain regions, especially over the western Pacific where salinity variation accounts for more than 20% of the sea level anomalies (Maes, 1998). Antonov et al. (2002) noticed that, in addition to the sea level change caused by temperature

variation, the input of fresh water into the ocean also contributed to sea level variations. We analyzed the effect of freshwater exchange by considering the precipitation minus evaporation ($P-E$) in the SCS. We computed evaporation rate from the latent heat flux because an accurate estimate of evaporation from observations was not available.

The evaporation (E) is given by

$$E = LHF/Lt \quad (5)$$

where LHF is the latent heat flux (W m^{-2}) and Lt the latent heat of vaporization, $Lt = 2.5 \times 10^6 \text{ J kg}^{-1}$.

The ($P-E$) is estimated for the SCS by taking the difference between the monthly mean precipitation derived from CMAP and the monthly mean evaporation that was computed from latent heat flux from NCEP. The ($P-E$) for the SCS domain is shown in Fig. 4. Besides the inter-annual variations associated with ENSO that resulted in a reduction of ($P-E$) in the SCS during the El Niño years, the long-term trend of the ($P-E$) was generally an increasing mode till 2000, but turned to a faster decreasing mode in 2001.

Cheng and Qi (2007) estimated the precipitation and evaporation rates in the SCS and found that precipitation exceeded evaporation by about 0.06–0.15 Sv/year ($1 \text{ Sv} = 10^6 \text{ m}^3 \text{ s}^{-1}$). Salinity variations were also caused by river discharge. The annual discharges of Pearl and Mekong rivers, the two major rivers in the SCS, are only 0.013 and 0.016 Sv, respectively. This is very small compared with the magnitude of ($P-E$). Fig. 4 shows that the trend of $P-E$ was in phase with the sea level anomalies and had a correlation coefficient of about 0.5 during 1997–2003. The $P-E$ contributed to the sea level rising at a rate of 1.5 mm/year from 1994 to 2000 and to the sea level falling at a rate of 4.8 mm/year afterwards. The rising rate in the sea level contributed by $P-E$ was one order of magnitude smaller than the observed rising rate of 11.3 mm/year and thus had a nominal contribution to sea level rise during this period. On the other hand, the falling rate contributed by $P-E$ was comparable to the sea level falling rate (6.03 mm/year) and contributed to about 80% of the sea level fall. Careful examination of correlation between ($P-E$) and sea level variations (Fig. 4 vs. Fig. 1)

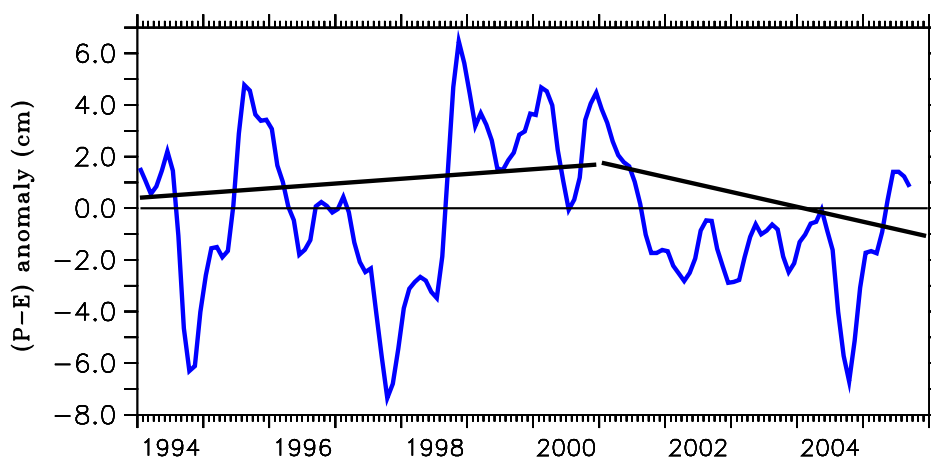


Fig. 4. Time evolution of ($P-E$) anomalies (cm) for the South China Sea domain.

indicated that the decrease of ($P-E$) started at January 2001, about 6 months ahead of sea level fall. This implies that the contribution of the ($P-E$) to the sea level change was small at the beginning of the regime shifting. Rong et al. (2007) also found that precipitation could have a significant effect on the sea level variability in the SCS during and after the mature phase of El Niño. Thus, it is clear from the above analysis that although the ($P-E$) could cause the sea level fall during the El Niño years, it alone could not explain the sea level variation in the SCS as shown in Fig. 1.

4.3. Sea level, net-heat flux, and SST from the model

To get a better understanding of the physical processes leading to the sea level shift in the SCS, we restricted our analysis to the period 1 July 2000–30 June 2003 when the sea level was highest and then fell dramatically causing a regime shift. The SLA from the high-resolution ocean model and the altimetry data for water depth greater than 200 m are shown in Fig. 5a. The dashed line represents the SLA from the model and the solid line represents anomalies from altimetry data for the period July 2000–June 2003.

To identify the dynamic and the thermodynamic forcing that are important in governing sea level variability in the SCS, we divided the time series into the warm phase when the SLA was higher and the cold phase when the SLA was lower. Since the sea level generally showed an increasing trend during September 2000–August 2001 and a decreasing trend from September 2001 to August 2002, the two time periods are defined as the warm and cold phases in the following discussion, respectively.

The net-heat flux from the model which represents the feedback effect of model's SST was compared with the net-heat flux computed from NCEP reanalysis and is presented in Fig. 5b. Both the fluxes were computed for water depths greater than 200 m in the SCS. The net-heat flux from NCEP data was computed using (4). The seasonal variability in the fluxes can be observed in the figure with both the model heat flux and the NCEP flux being higher during March–May before the onset of the southwest monsoon winds. During this time, the sky over the SCS was relatively clear with less cloud cover and rainfall, and, thus, more shortwave radiation entered into the upper layer of the ocean (Wang and Wang, 2006). Owing to the weak winds, the loss of latent heat flux from the ocean was also low and both of these factors caused a seasonal maximum in net-heat flux during March–May and vice

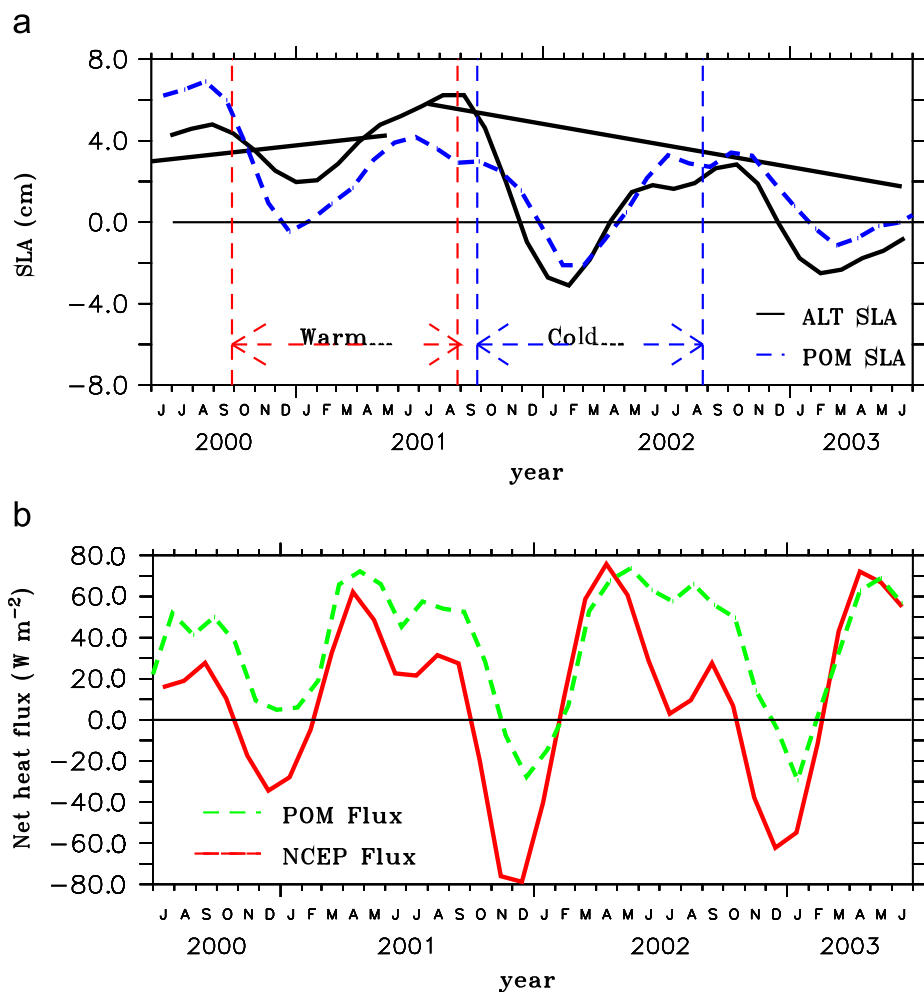


Fig. 5. (a) Time evolution of sea level anomalies (cm) and (b) net-heat flux anomalies ($W m^{-2}$) for the South China Sea domain. Dashed line represents the anomalies of net-heat flux and sea level from the model.

versa during December–January. A striking feature in the net-heat flux variation was the sharp decrease in the heat flux during December 2001 both in the model and NCEP when the sea level started to fall in the SCS.

The spatial pattern of net atmospheric heat flux during the warm and cold phases are presented in Fig. 6. The positive values represent gain of heat by the ocean and negative values the loss by the ocean. The net-heat flux was positive in the southern SCS and was negative in the northern part during both the warm and the cold phases. However, during the cold phase, a considerably larger magnitude of heat loss (negative value) occurred over the northern part of the SCS. The gain of heat represented by

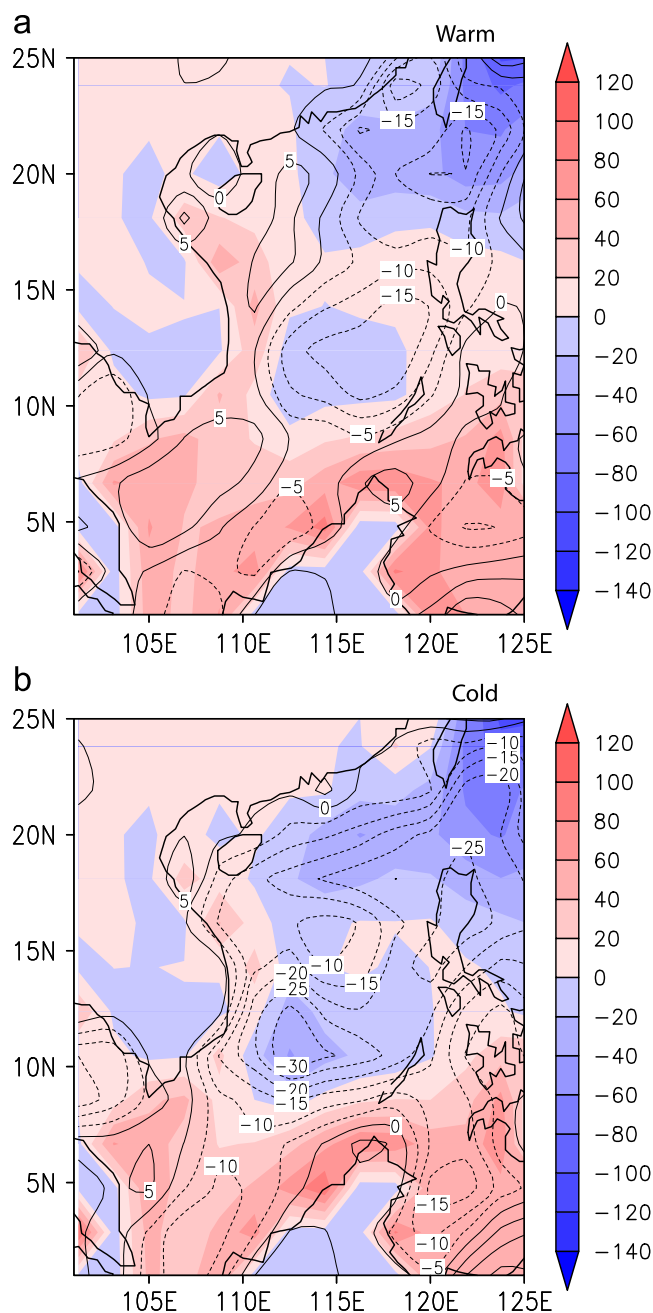


Fig. 6. Spatial distribution of net-heat flux (W m^{-2} , shaded) from NCEP reanalysis data: (a) warm phase (September 2000–August 2001). (b) Cold phase (September 2001–August 2002). The contour lines represent net-heat flux anomalies.

the positive values in the southern part of SCS also decreased during the cold phase in comparison with the warm phase. Thus, there was a net reduction in the net atmospheric heat flux from the warm to the cold phase in the SCS.

The sea surface temperature from the MODIS and model during the warm and cold phases are shown in Fig. 7. The SST during the warm phase was more than 30°C in the southern SCS, in the Gulf of Thailand and to the west of Luzon Islands. The Kuroshio was indicated by the warm water track both in the model and observation, while cold SST (below 24°C) is seen in the northern part of the SCS and in the Taiwan Strait. However, during the cold phase, the SST decreased and generally lower values were seen in the SCS (Figs. 7c and d), particularly in the regions west of Luzon and in the southern SCS. The lower SST north of 22°N further decreased during the cold phase. Another important feature was the decrease in the temperature of the Kuroshio and the western Pacific during the cold phase. The decrease in the net atmospheric heat flux from warm to cold phase has contributed to the decrease of SST during the cold phase. The SST from the model was found to be generally lower than the MODIS SST, but had major characteristics of variations similar to the MODIS SST during both the warm and the cold phases.

4.4. Western Pacific warm pool and sea level variations in the SCS

4.4.1. SST and heat content

The SCS is located within the area of the Indo-Pacific warm pool that anchors the largest atmospheric convection center. The 28°C isotherm is often chosen as the boundary for the warm pool. Because the SST in the SCS during the warm and cold phases showed considerable difference consistent with the temperature changes observed in the western Pacific warm pool, we have analyzed the SST in the Indo-Pacific warm pool from MODIS data (Fig. 8). The Indo-Pacific warm pool is a region of critical importance for the development of ENSO events which, to a large degree, involves zonal displacements of the warm pool and the location of atmospheric convection (Philander, 1990). Fig. 8 shows warm SST anomalies (SSTA) in the western Pacific and in the SCS during the warm phase. Positive SSTA were seen across the Luzon Strait, in the southeastern SCS, and near the Karimata Strait. However, during the cold phase the western Pacific and the SCS were covered mainly by the negative SSTA.

Similar trends were also reflected in the subsurface temperature anomalies (SOT). The domain-averaged temperature anomalies as a function of water depth from SODA for the SCS (100°E – 120°E , 0° – 22°N) and equatorial western Pacific (120°E – 140°E , 10°S – 10°N), (indicated by boxes in Fig. 8b) during the warm and cold phases are shown in Fig. 9a. The temperature profiles show general positive/negative anomalies of temperature in the water column in both the western Pacific and the SCS during the warm/cold phase. In particular, the largest positive

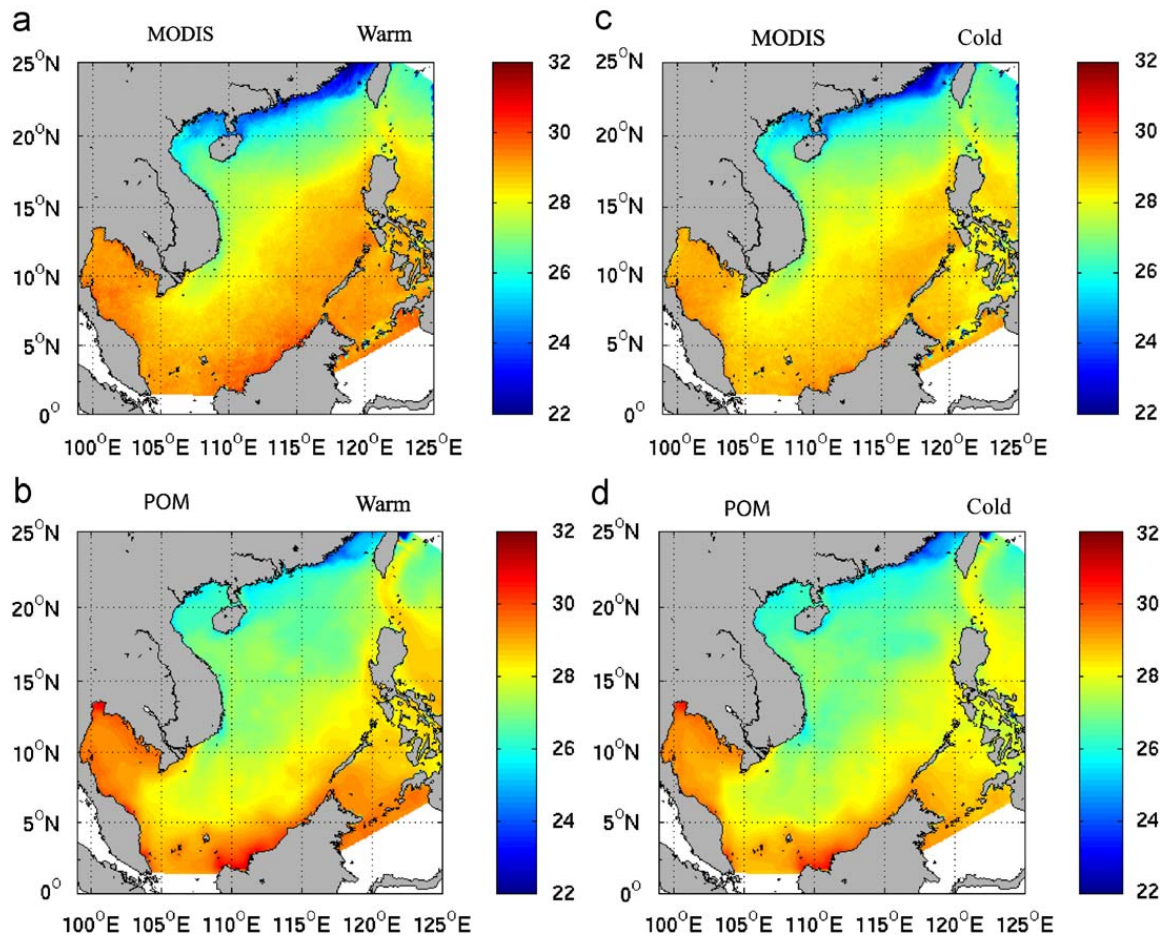


Fig. 7. Sea surface temperature (°C) from MODIS and model: (a, b) warm phase (September 2000–August 2001). (c, d) Cold phase (September 2001–August 2002).

temperature anomalies occurred around 100 m depth during the warm phase both inside and outside of the SCS. However, the largest negative temperature anomalies centered at 150 m in the western Pacific and 50 m in the SCS during the cold phase.

Li and Mu (1999) studied the SOT in the western Pacific warm pool and the occurrence of ENSO. They found presence of positive (negative) SOT in the western Pacific prior to the occurrence of El Niño (La Niña) and these positive (negative) anomalies were replaced by negative (positive) SOT during the developing and mature stages of El Niño (La Niña). The study by Zhang and Levitus (1997) also reported the presence of negative (positive) SOT in the western tropical Pacific during El Niño (La Niña) years. The longitude-time plot of SOT at 100 m depth for the equatorial western Pacific and SCS is shown in Fig. 9b. The warm and cold phases are also marked in the figure. During the developing and mature stages of El Niño in 1997 and 2002, negative SOT were present in the equatorial western Pacific, but during La Niña years (between 1998 and 2001), positive SOT were seen. It is interesting to note that the pattern of SOT in the SCS was generally similar to that in the western Pacific, particularly during the warm and cold phases.

The warm SOT in the equatorial western Pacific prior to the El Niño builds up high heat content. Eastward migration of the western Pacific warm pool with en-

hanced heat content anomalies (*HCA*) during the development stages of the 1997 El Niño event was discussed by McPhaden (1999). Negative heat content anomalies were observed in the western Pacific when the El Niño matures. In the off-equatorial band there was westward propagation of heat content anomalies from the eastern Pacific following the El Niño and La Niña events (Zebiak, 1989; Kirtman, 1997). These are associated with the off-equatorial Rossby waves found in the latitudinal band poleward of 6°N from the equator during the ENSO episodes. Following the La Niña event, negative *HCA* propagate westwards, while following the El Niño event, positive *HCA* propagate westwards. The propagation of the off-equatorial *HCA* is presented in Fig. 10. The *HCA* in the upper 300 m of the water column were computed from SODA as follows:

$$HCA = \rho C_p \int_0^{300} (T - T_{clim}) dz \quad (6)$$

where ρ is the density of the water column ($\rho = 1000 \text{ kg m}^{-3}$), and C_p the specific heat capacity of water ($C_p = 4186 \text{ J kg}^{-1} \text{ K}^{-1}$). T is the temperature of the water column, and T_{clim} the mean climatological temperature. The *HCA* is averaged in the off-equatorial band between 10°N and 20°N. It can be seen that following the 1997 El Niño, positive *HCA* propagated westwards and reached the western boundary during 1998. These positive *HCA*

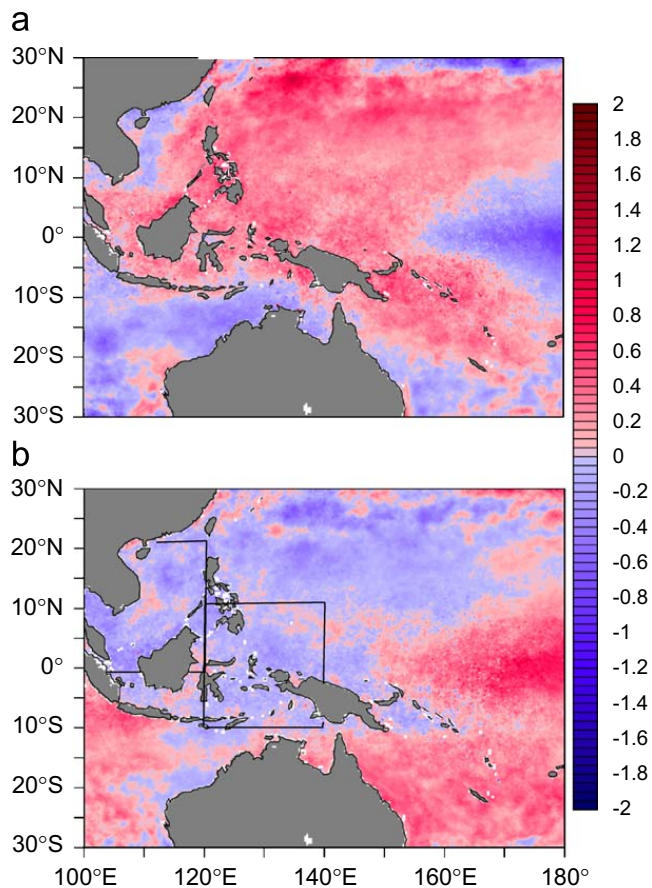


Fig. 8. Sea surface temperature anomaly ($^{\circ}\text{C}$) from MODIS: (a) warm phase (September 2000–August 2001). (b) Cold phase (September 2001–August 2002). The boxes in (b) represent the SCS and Pacific domain used for averaging the subsurface temperature in Fig. 9.

persisted in the off-equatorial western Pacific till 2001, which corresponded to the warm phase in the SCS, while during the cold phase following the La Niña year, a negative *HCA* persisted in the western Pacific.

The ENSO signal from the western Pacific is transmitted into the SCS through the western boundary current, the Kuroshio, which flows poleward north of 10°N in the western Pacific. During the La Niña period (1998–2001), the heat content in the western Pacific was higher and the intrusion of Kuroshio transported warmer water into the SCS through the Luzon Strait. With the increase in the heat advection from the Pacific, the heat content in the SCS was increased and sea level rose during that period, while during the cold phase (El Niño years) the heat advection from the Pacific was lowered. The heat transport across the Luzon Strait is examined in detail using the high-resolution ocean general circulation model and is presented in Section 4.2. These results suggest that the warm and cold phases in the SCS were highly correlated with the western Pacific subsurface temperature.

4.4.2. Heat content anomalies and steric sea level variation

The strong influence of the subsurface temperatures of the western Pacific in the SCS can be seen in the

horizontal distribution of annual mean *HCA* (Fig. 11a), obtained from SODA data covering both the SCS and the western Pacific. The *HCA* were averaged for the warm and cold phases, respectively. During the warm phase, strong positive *HCA* were seen in the western Pacific and the Kuroshio region. There was an extension of these positive *HCA* from the western Pacific through the Luzon Strait into the SCS which connected with the positive *HCA* in the central and northern parts of the SCS. However, negative *HCA* were seen in the southern part near the Karimata Strait. The difference in the *HCA* between the warm and cold phases is presented in Fig. 11b. The positive values of difference between warm and cold phases seen in the western Pacific, the Luzon Strait and SCS clearly indicated an excess of warming in these regions and the linkage among them during the warm phase.

The changes in the heat content of the ocean caused the steric variability of sea level (Gill and Niiler, 1973). The steric sea level anomalies were computed using Eq. (2) and are shown in Fig. 11c for the warm phase. The steric sea level anomalies resemble the heat content anomalies with large steric height variation in the Kuroshio region of western Pacific near Luzon Strait and in the SCS during the warm phase. The difference in the steric sea level variation between warm and cold phases (Fig. 11d) showed that the steric height anomalies were greater in the SCS during the warm phase than during the cold phase. These are in agreement with the corresponding steric height variations in the western Pacific region.

The above analysis gives a broad picture of the effect of subsurface temperature anomalies in the western Pacific on the sea level variability in the SCS. The Pacific water enters into the SCS through the Luzon Strait. The strait has a width of about 350 km and hence we need high-resolution data to resolve the volume transport in order to quantify the intrusion of warm Pacific water and its contribution to sea level variability in the SCS. For this purpose we used the high-resolution regional ocean model to investigate the influence of heat advection on the variability in the SCS.

The SLA and the *HCA* from the high-resolution SCS model for the warm and the cold phases are presented in Fig. 12. The SLA showed a rise in sea level near the Luzon Strait, west of the Luzon Strait and in the central part of the SCS during the warm phase. The pattern of SLA was consistent with the heat content anomalies during the warm phase. The heat content in the SCS was higher in the eastern and central parts of the SCS. However, during the cold phase, large negative SLA and *HCA* were found in the eastern and central parts of SCS. Thus, between the warm and the cold phases, the heat content underwent a dramatic shift in the SCS.

4.5. Heat budget of the South China Sea

To further understand the sea level variations caused by changes in the net atmospheric heat flux and/or the heat advection, it is helpful to analyze the heat budget in the SCS during the warm and the cold phases. The volume ($Q_v, \text{m}^3 \text{s}^{-1}$) and heat transport ($Q_T, \text{m}^3 \text{s}^{-1} \text{ } ^{\circ}\text{C}$) through the

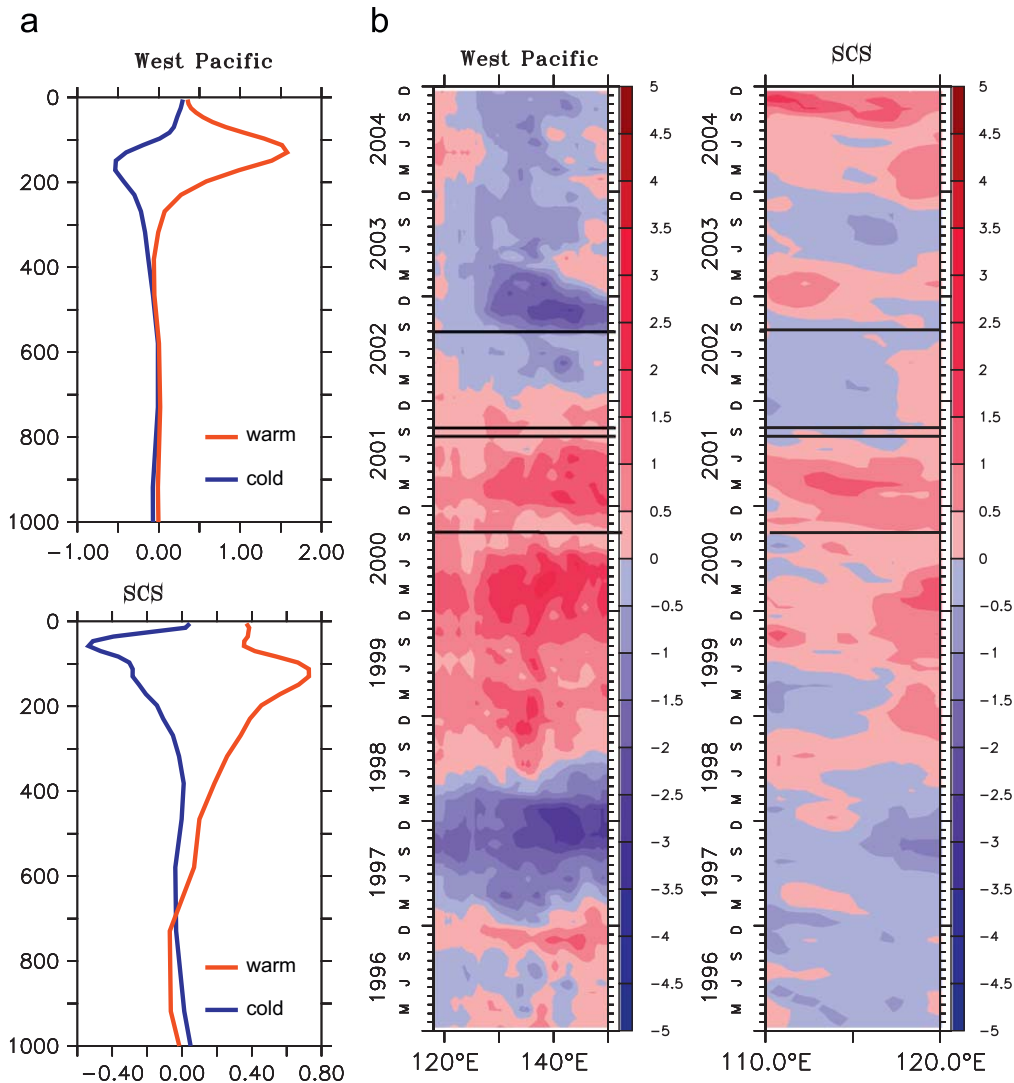


Fig. 9. (a) Vertical distribution of subsurface temperature anomalies ($^{\circ}\text{C}$) for the western Pacific warm pool region and South China Sea. (b) Subsurface temperature anomaly ($^{\circ}\text{C}$) at 100 m depth averaged between 10°S and 10°N for the western Pacific and 0°N and 20°N for the South China Sea. The warm and cold phases are marked in the figure. The data are from SODA.

Luzon Strait were estimated using the formula

$$Q_V = \int_A U dA \quad (7)$$

where A is the cross-sectional area across the Luzon Strait and U the zonal velocity (m s^{-1}):

$$Q_T = \int_A UT dA \quad (8)$$

where T is the temperature ($^{\circ}\text{C}$) across the Luzon Strait.

Fig. 13 shows the volume and heat transport across the Luzon Strait during the warm and cold phases from the high-resolution regional model. Many studies using both hydrographic data analyses and numerical modeling showed that intrusion of north Pacific water into the SCS occurs throughout the year (Qiu et al., 1984; Guo, 1985; Qu et al., 2004; Gan et al., 2006) with the relatively strong Kuroshio branch flowing westward through the Luzon Strait in winter and early spring. The vertical structure of

Luzon Strait transport consists of inflow and outflow regions (Qu et al., 2004; Tian et al., 2006). The inflow region where Pacific water intrudes into the SCS extends from the surface to about 600 m. The outflow region is between 600 m depth and 1000 m depth. The region below 1000 m is again characterized by inflow of Pacific water. The transport through the Luzon Strait derived from the model very successfully reproduced the vertical structure of the flow pattern, which is very important in understanding the heat budget of the SCS. It can be seen from Fig. 13a that more inflow of Pacific water into the SCS took place in the upper 400 m during the cold phase which coincided with El Niño. The transport from surface to 400 m was estimated to be 1.4 Sv during the cold phase and 0.64 Sv during the warm phase. This is consistent with the study of Qu et al. (2004). They found more Luzon Strait transport during El Niño years and less during La Niña years, i.e., more Pacific water entered into the SCS during the cold phase. The fact that the sea level in the SCS was higher during the warm phase and was lower during the

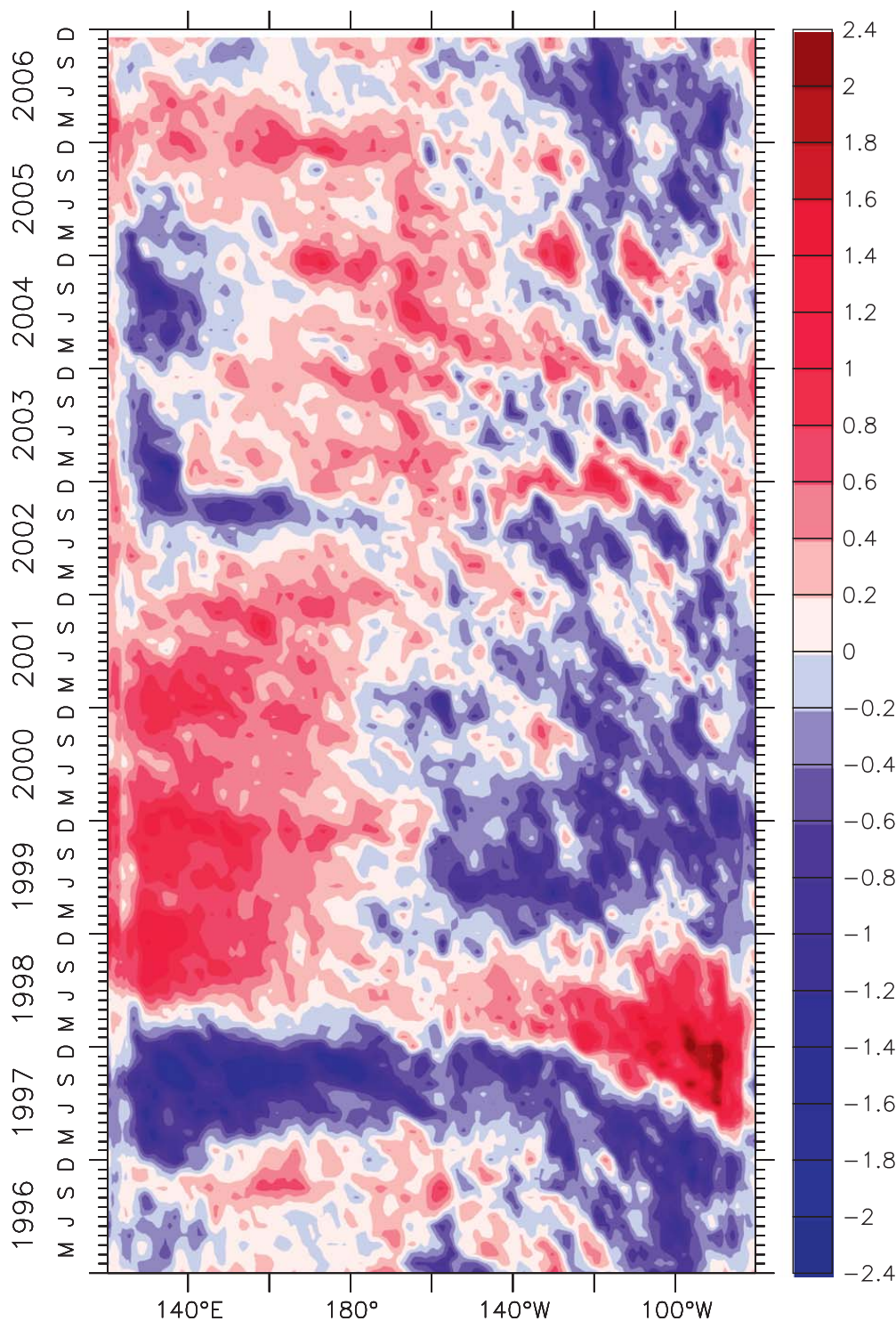


Fig. 10. Heat content anomaly ($\times 10^9 \text{J m}^{-2}$) in the upper 300 m for the off-equatorial Pacific Ocean between 10°N and 20°N . The data are from SODA.

cold phase suggests a role other than the net mass transport from the Pacific into the SCS in affecting the sea level change between warm and cold phases. The mechanism is demonstrated in the following analysis of heat transport through Luzon Strait.

The heat transport through the Luzon Strait and the heat transport difference between the warm and the cold phases (warm phase minus cold phase) is shown in

Figs. 13c and d. The red line represents the heat transport during the warm phase and the blue line represents heat transport during the cold phase. Heat transport was estimated by (8) across the Luzon Strait during the warm and cold phases. It can be seen from Fig. 13c that the heat transport was larger during the warm phase than during the cold phase. During the warm phase (La Niña) the western Pacific was warmer than normal and the Kuroshio

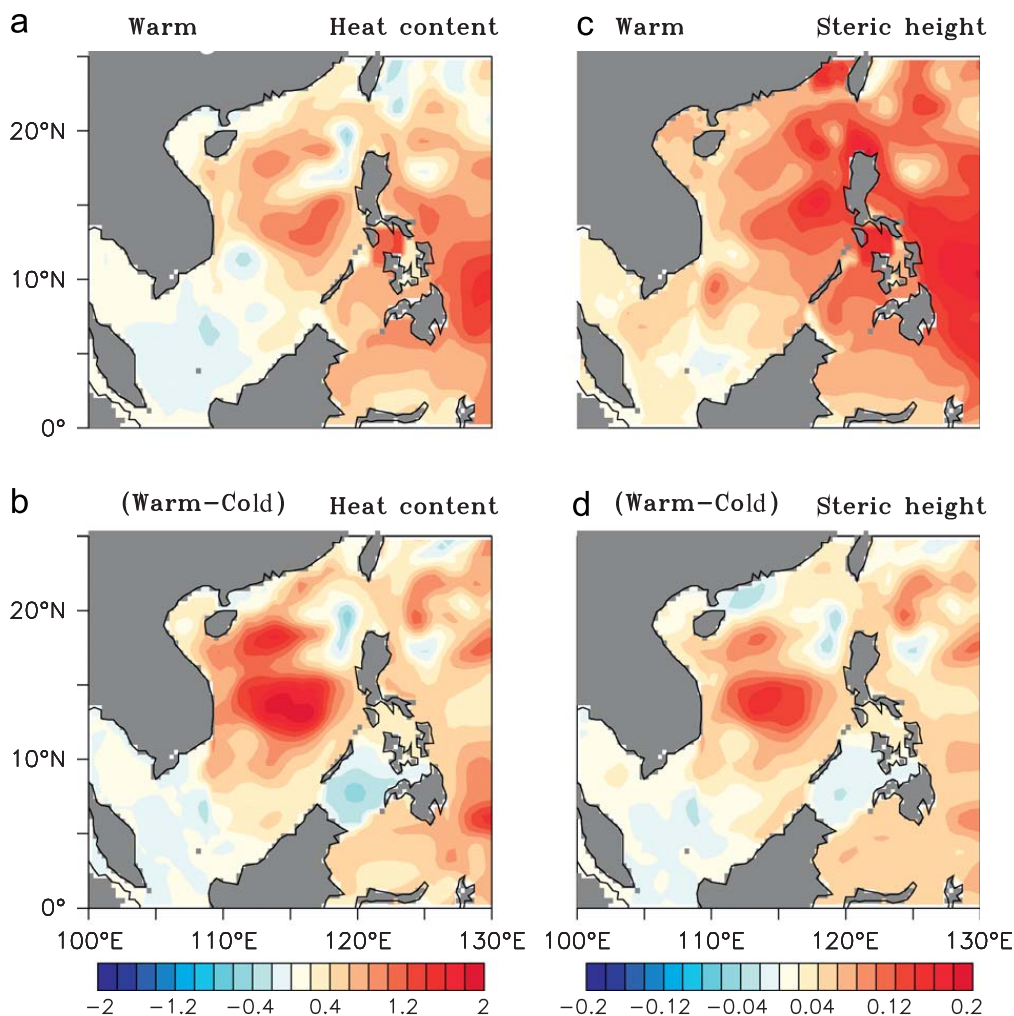


Fig. 11. (a) Anomalies of heat content ($\times 10^9 \text{J m}^{-2}$) during warm phase (September 2000–August 2001). (b) Difference between warm and cold (September 2001–August 2002) phase. (c, d) Same as above except for steric height anomalies. The data are from SODA.

transported warmer water into the SCS, while during the cold phase (El Niño) the heat entering the SCS was considerably reduced. Rong et al. (2007) noticed more volume transport through Luzon Strait during El Niño years, but they also found more outflow through the Mindoro Strait during July–September to compensate for the increased volume transport during the El Niño years. Nevertheless their study did not realize the significant warm water penetration from the Pacific into the SCS during La Niña years.

The Luzon Strait is the only deep channel that connects the SCS with the Pacific and the transport across the Luzon Strait is the greatest compared with transport through the Mindoro and Balabac Straits which connect the SCS to the Sulu Sea. Qu et al. (2006) discussed the SCS throughflow and they found that, on annual average, the waters exiting through the Karimata and Mindoro Straits were warmer by about 1.8°C than that entering through the Luzon Strait. The heat flux was found to be positive in the southern SCS (Fig. 6). This makes the water leaving the SCS warmer than at entering it. However, Qu et al. (2006) also noticed inter-annual variability whereby the SCS received an excess of heat during La Niña years. In the

model used for the present study, the total mass was conserved. The water entering the SCS was balanced by the mass leaving SCS. During the warm phase the volume transport across the Luzon Strait was less than it was during the cold phase. Hence, less water exits the SCS with a higher temperature in the south than during the cold phase. Also, the water entering the SCS from Pacific was warmer than the cold phase. This raises the sea level in the SCS during the warm phase. To get a clear idea about the contribution of net atmospheric heat flux and heat advection to the warm (sea level rise) and cold (sea level fall) phases in the SCS, we analyzed the depth-integrated potential temperature equation.

In the depth-integrated temperature equation, the rate of change of temperature (dT/dt) is balanced by the net atmospheric heat flux (Q) and heat advection (Adv). The dT/dt represents the changes in heat content of the water column with time in the SCS. The time series of heat content from the model and SODA are shown in Fig. 14a and b, respectively. The heat content was higher during 2000 and then it showed a slow decrease during the warm phase followed by a rapid decrease during the cold phase. The warmer water advection from the western Pacific into

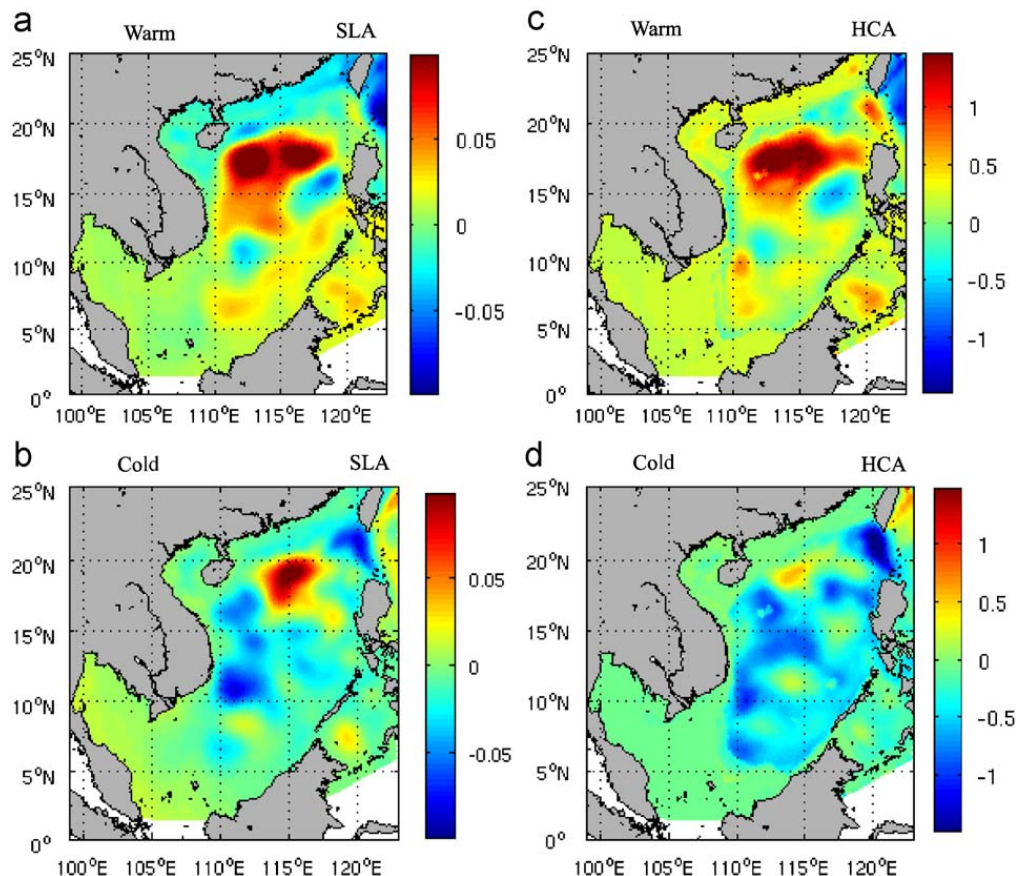


Fig. 12. Anomalies of sea level (cm) and heat content ($\times 10^9 \text{ J m}^{-2}$) from the model: (a, c) warm phase (September 2000–August 2001). (b, d) Cold phase (September 2001–August 2002).

the SCS during the La Niña period raised the heat content of the water column resulting in thermal expansion and sea level rise in the SCS.

The terms from the temperature equation averaged for the SCS domain for water depth more than 200 m are shown in Fig. 15. The terms are presented after removal of the semi-annual cycle. The details of the term derivations in the temperature equation can be seen in Gan and Allen (2005a) and are also presented in the appendix. The advection terms, written in conservation form in the POM, are rewritten to remove the contribution of the continuity equation. The dT/dt (black line) showed similar pattern of variation as the heat content and was larger during the beginning of the warm phase. The dT/dt is balanced by the net atmospheric heat flux (red line) and heat advection (blue line). The SCS gained heat from the atmospheric during the warm phase and was balanced by the cold advection. During the shifting of warm to the cold phase, net atmospheric heat flux decreased and hence cold advection also decreased. The dT/dt also decreased accordingly. More water with lower temperature entered the SCS and more water with a higher temperature left the SCS in the south during the cold phase. Thus cold advection increased and further decrease of dT/dt during the cold phase was caused by cold water advection as shown by higher positive values of advection during later stages of the cold phase. The temperature equation reveals

that the shift from warm to cold phase was caused by the reduction of net atmospheric heat flux and the cold phase was maintained by the cold advection in the SCS.

5. Summary

Global warming is underway and the sea level in the global oceans is rising. Though many studies have addressed the global sea level variations, the physical processes leading to regional sea level variations are yet to be understood. The sea level in the SCS showed an increase followed by a sudden decrease during 2000–2003. The cause of this observed shift in sea level and, hence, the warm/cold phases in the SCS, are not well-understood. This lack of understanding was caused by uncertainty in the mass and heat transport through the narrow straits that connect the SCS to the surrounding seas and to the Pacific Ocean. We calculated the heat budget using a high-resolution model and analyses of remote sensing and other available data were carried out to investigate the observed variability in the sea level during 2000–2003 in the SCS.

The variation in sea level represents a combination of changes of which the steric sea level variation and net water mass change either through ($P-E$) or through the exchange between the SCS and adjacent seas and Pacific

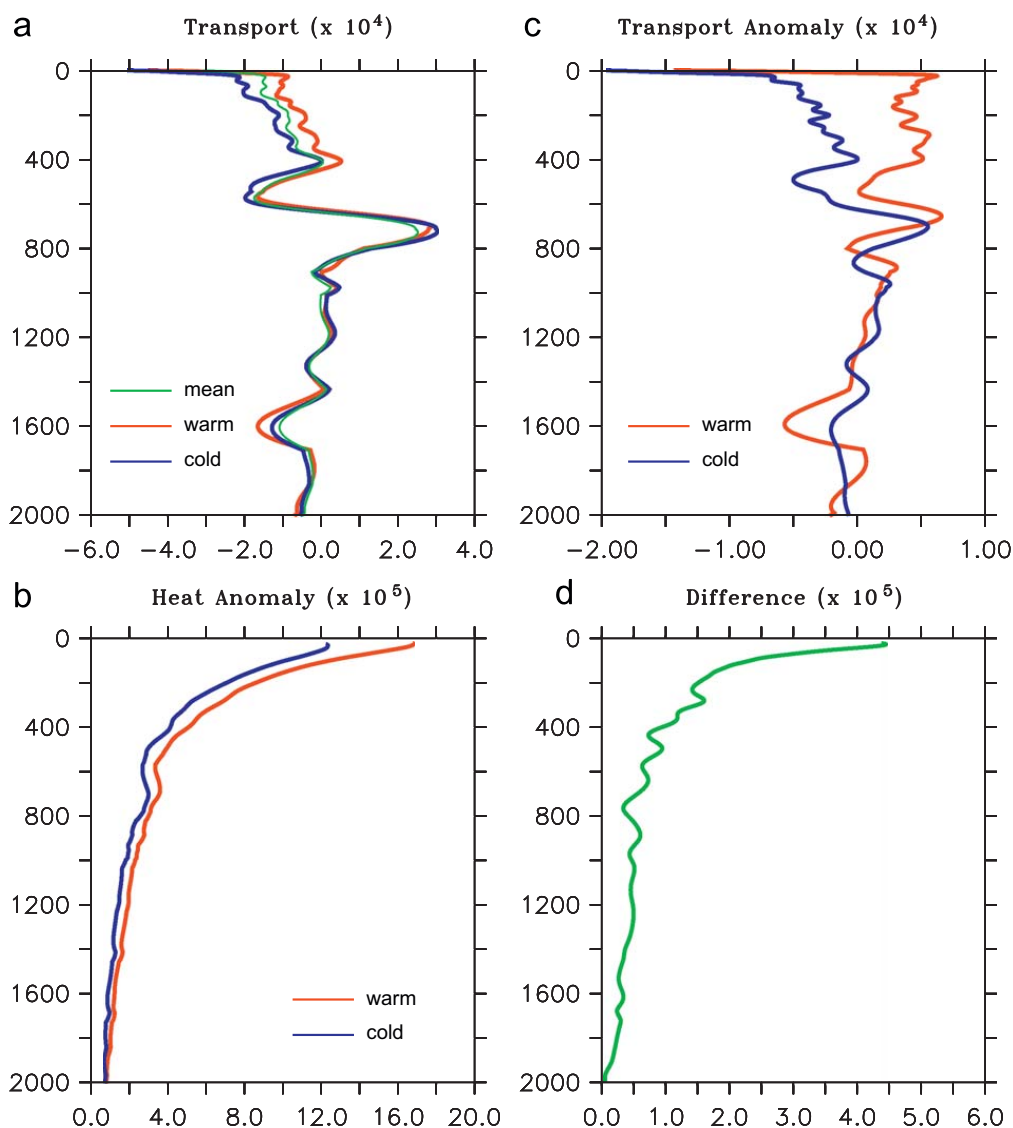


Fig. 13. (a) Volume transport through the Luzon Strait ($\times 10^4 \text{ m}^3 \text{ s}^{-1}$). (b) Transport anomaly ($\times 10^4 \text{ m}^3 \text{ s}^{-1}$). The volume transport is estimated for each meter of the water column. The negative values represent the westward flow (inflow) and the positive values represent the eastward flow (outflow). (c) Heat flux anomalies ($\times 10^4 \text{ m}^3 \text{ s}^{-1} \text{ }^\circ\text{C}$) through the Luzon Strait. (d) Difference in heat flux anomalies ($\times 10^4 \text{ m}^3 \text{ s}^{-1} \text{ }^\circ\text{C}$).

Ocean, influenced by El Niño/La Niña episodes in the Pacific, are found to be important in affecting sea level variation in the SCS. Both the convergence/divergence of mass and the SST did not show any coherent trend with the sea level variation. To identify the dynamic and thermodynamic forcing that were important in governing sea level variability, we divided the time series into the warm phase when sea level was higher (from September 2000 to August 2001), and the cold phase when the sea level was lower in the SCS (from September 2001 to August 2002).

The warm phase was associated with the transition period from La Niña to El Niño and the cold phase was associated with El Niño. The temperature in the western Pacific was observed to be warmer than normal during La Niña years and cooler than normal during El Niño years. The SCS is located in the Indo-Pacific warm pool and the variation of temperature in the western Pacific influenced the temperature and sea level in the SCS. During the warm phase (La Niña), warmer water from the western Pacific

entered the SCS through the Luzon Strait. The water entering the SCS was largely balanced by the mass leaving the SCS. The volume transport through the Luzon Strait was found to be less during the warm phase than during the cold phase and hence less water exited the SCS with a higher temperature in the south during the warm phase. These raised the sea level in the SCS during the warm phase. The net atmospheric heat flux decreased from warm to cold phase. The analysis revealed that the shift from the warm to the cold phase in the SCS is triggered by the reduction in the net atmospheric heat flux and maintained by cold water advection. The decrease of ($P-E$) during the cold phase in association with El Niño also played a significant role in the falling of sea level during the cold phase. With the increasing trend of the heat content in the western Pacific in the Kuroshio region and the future intense and persistent El Niño events revealed by the IPCC projections, the present study is important in understanding the sea level variations in the SCS.

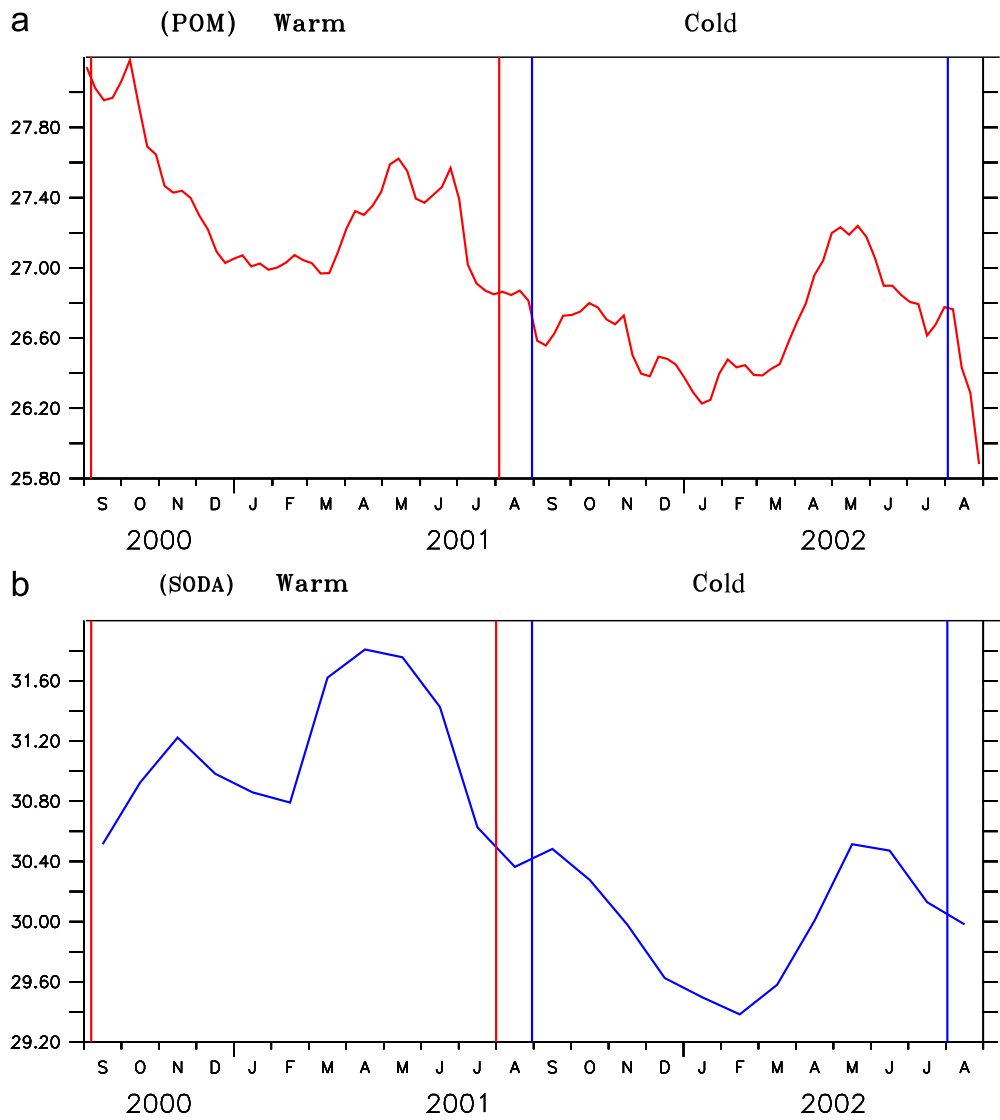


Fig. 14. Time evolution of heat content ($\times 10^9 \text{J m}^{-2}$) from the model and SODA.

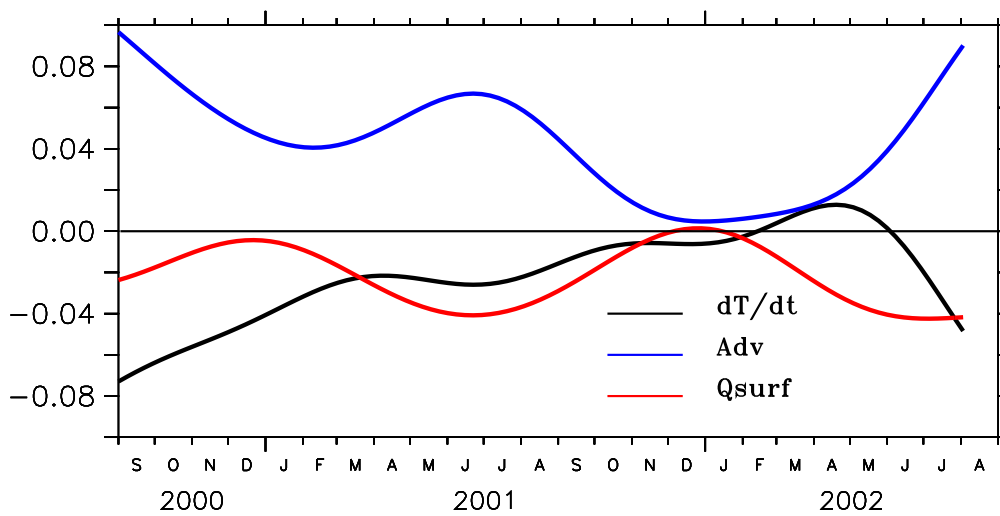


Fig. 15. Time series of terms in depth-averaged temperature equation ($^{\circ}\text{C s}^{-1}$, multiplied by 10^{-7}) calculated from the model. The terms are presented after removal of the semi-annual cycle.

Acknowledgments

This research was supported by the National Key Basic Research Development Program 2009CB421208, the Research Grants Council of Hong Kong under Grant nos. CERG-601006 and RPC07/08.SC12. The authors thank the editor and the three anonymous reviewers for their valuable suggestions.

Appendix

The depth-integrated equation for potential temperature (Gan and Allen, 2005a) is

$$\int_{-1}^0 \frac{\partial \theta D}{\partial t} d\sigma + \int_{-1}^0 \frac{\partial \theta u D}{\partial x} d\sigma + \int_{-1}^0 \frac{\partial \theta v D}{\partial y} d\sigma + \int_{-1}^0 \frac{\partial \theta \omega}{\partial \sigma} d\sigma - \int_{-1}^0 \frac{\partial}{\partial \sigma} \left(\frac{K_H \partial \theta}{D} \right) d\sigma - \int_{-1}^0 F_\theta d\sigma - \int_{-1}^0 \frac{\partial R}{\partial \sigma} d\sigma = 0 \quad (\text{A.1})$$

where θ is the potential temperature, $D = H + \eta$ the water depth, H the undisturbed water depth, η the surface elevation, K_H the vertical diffusivity, F_θ the horizontal diffusion, and R the shortwave radiation flux.

The nonlinear advection terms are written in conservative (or divergence) form

$$DADV = \int_{-1}^0 \frac{\partial \theta u D}{\partial x} d\sigma + \int_{-1}^0 \frac{\partial \theta v D}{\partial y} d\sigma + \int_{-1}^0 \frac{\partial \theta \omega}{\partial \sigma} d\sigma \quad (\text{A.2})$$

To evaluate the relative contribution of alongshore and across-shore temperature advection, it is necessary to remove the terms in the continuity equation from (A.2). The balanced equation is of the form

$$\frac{\partial u D}{\partial x} + \frac{\partial v D}{\partial y} + \frac{\partial \omega}{\partial \sigma} = 0 \quad (\text{A.3})$$

The depth-averaged form of (A.3) is

$$\frac{\partial U_b D}{\partial x} + \frac{\partial V_b D}{\partial y} = 0 \quad (\text{A.4})$$

The individual advection terms are rewritten as

$$DADVY = \int_{-1}^0 \left(\frac{\partial \theta v D}{\partial y} - \theta \frac{\partial V_b D}{\partial y} \right) d\sigma \quad (\text{A.5})$$

$$DADVX = \int_{-1}^0 \left(\frac{\partial \theta u D}{\partial x} - \theta \frac{\partial U_b D}{\partial x} \right) d\sigma \quad (\text{A.6})$$

As a result of the boundary condition $\omega = 0$ at $\sigma = 0, -1$, the last term on the right-hand side of (A.2) is zero so that with (A.4),

$$DADV = DADVY + DADVX \quad (\text{A.7})$$

The advection terms can be written as

$$ADVY_1 = H^{-1} DADVY \quad (\text{A.8})$$

$$ADVX_1 = H^{-1} DADVX \quad (\text{A.9})$$

The rate of change of temperature,

$$\frac{dT}{dt} = H^{-1} \left(\int_{-1}^0 \frac{\partial \theta D}{\partial t} \right) d\sigma \quad (\text{A.10})$$

$$Q_{surf} = -H^{-1} \left(\int_{-1}^0 \frac{\partial}{\partial \sigma} \left(\frac{K_H \partial \theta}{D} \right) d\sigma + \int_{-1}^0 \frac{\partial R}{\partial \sigma} d\sigma \right) \quad (\text{A.11})$$

Where $DADVY$ and $DADVX$ are given by (A.5) and (A.6), respectively, and where we assume H approximately equals D .

The spatial distribution of the time-averaged terms is calculated in the following manner, where an angle bracket denotes a time average over the time interval $t_f = t_2 - t_1$:

$$\left\langle \frac{dT}{dt} \right\rangle = t_f^{-1} \int_{t_1}^{t_2} \frac{dT}{dt} dt \quad (\text{A.12})$$

$$\langle Q_{surf} \rangle = t_f^{-1} \int_{t_1}^{t_2} Q_{surf} dt \quad (\text{A.13})$$

$$\langle ADVX_1 \rangle = t_f^{-1} \int_{t_1}^{t_2} ADVX_1 dt \quad (\text{A.14})$$

$$\langle ADVY_1 \rangle = t_f^{-1} \int_{t_1}^{t_2} ADVY_1 dt \quad (\text{A.15})$$

References

- Antonov, J.I., Levitus, S., Boyer, T.P., 2002. Steric sea level variations during 1957–1994. Importance of salinity. *J. Geophys. Res.* 107 (C12), 8013.
- Antonov, J.I., Levitus, S., Boyer, T.P., 2005. Thermosteric sea level rise, 1955–2003. *Geophys. Res. Lett.* 32, L12602.
- Bosch, A., et al., 2006. Coastal Sea Surface Topography—A Synthesis of Altimetry, Gravity, and Tide Gauges, Aviso Newsletter, vol. 11. CNES, Toulouse.
- Blumberg, A.F., Mellor, G.L., 1987. A description of a three-dimensional coastal ocean circulation model. In: Heaps, N. (Ed.), *Three-dimensional Coastal Ocean Models*, Coastal Estuarine Series, vol. 4. AGU, Washington, DC, pp. 1–16.
- Carton, J.A., Chepurin, G., Cao, X., Giese, B., 2000. A simple ocean data assimilation analysis of the upper ocean 1950–95. Part I: methodology. *J. Phys. Oceanogr.* 30, 294–309.
- Carton, J.A., Giese, B., Grodsky, S.A., 2005. Sea level rise and the warming of the oceans in the Simple Ocean Data Assimilation (SODA) ocean reanalysis. *J. Geophys. Res.* 110, C09006.
- Cazenave, A., Nerem, R.S., 2004. Present-day sea level change: observations and causes. *Rev. Geophys.* 42, RG3001.
- Cheng, X., Qi, Y., 2007. Trends of sea level variations in the South China Sea from merged altimetry data. *Global Planet. Sci.* 57 (3–4), 371–382.
- Church, J., Gregory, J.M., Huybrechts, P., Kuhn, M., Lambeck, K., Nhuan, M.T., Qin, D., Woodworth, P.L., 2001. Changes in sea level. In: Houghton, J.T., et al. (Eds.), *Climate Change 2001: The Scientific Basis*, Contribution of Working Group I to the Third Assessment Report of the Intergovernmental Panel on Climate Change. Cambridge University Press, New York, pp. 639–693.
- Curchitser, E.N., Haidvogel, D.B., Hermann, A.J., Dobbins, E.L., Powell, T.M., Kaplan, A., 2005. Multi-scale modeling of the North Pacific Ocean: assessment and analysis of simulated basin-scale variability (1996–2003). *J. Geophys. Res.* 110, 11021.
- Fang, W., Guo, J., Shi, P., Mao, Q., 2006. Low frequency variability of South China Sea surface circulation from 11 years of satellite altimeter data. *Geophys. Res. Lett.* 33, L33612.

- Gan, J., Li, H., Curchitser, E.N., Haidvogel, D.B., 2006. Modeling South China Sea circulation. Response to seasonal forcing regimes. *J. Geophys. Res.* 111, C06034.
- Gan, J., Allen, J.S., 2005a. Modeling upwelling circulation of the Oregon coast. *J. Geophys. Res.* 110, C10S07.
- Gan, J.P., Allen, J.S., 2005b. On open boundary conditions in a limited-area coastal model off Oregon: response to idealized wind forcing. *Ocean Modelling* 8, 115–133.
- Gan, J., Allen, J.S., Samelson, R., 2005. On open boundary conditions for a limited-area coastal model off Oregon. Part 2: response to wind forcing from regional mesoscale atmospheric model. *Ocean Modelling* 8, 155–173.
- Gill, A.E., Niiler, P.P., 1973. The theory of the seasonal variability in the ocean. *Deep-Sea Res.* 20, 141–177.
- Gregory, J.M., et al., 2001. Comparison of results from several AOGCMs for global and regional sea-level change 1900–2100. *Climate Dyn.* 18, 225–240.
- Guo, Z., 1985. Wintertime South China Sea Warm Current and the westward current on its right. *Trop. Oceanol.* 4, 1–9 (in Chinese with English abstract).
- Ho, C.R., Zheng, Q., Soong, Y.S., Kuo, N.J., Hu, J.H., 2000. Seasonal variability of sea surface height in the South China Sea observed with TOPEX/Poseidon altimeter data. *J. Geophys. Res.* 105 (C6), 13981–13990.
- Holgate, S.J., Woodworth, P.L., 2004. Evidence for enhanced coastal sea level rise during the 1990s. *Geophys. Res. Lett.* 31, L07305.
- Ishii, M., Sakamoto, K., Iwasaki, S., 2006. Steric sea level changes estimated from historical ocean subsurface temperature and salinity analyses. *J. Oceanogr.* 62 (2), 155–170.
- Kang, S.K., Cherniawsky, J.Y., Foreman, M.G.G., 2005. Patterns of recent sea level rise in the East/Japan Sea from satellite altimetry and in situ data. *J. Geophys. Res.* 110, C07002.
- Kistler, R., et al., 2001. The NCEP/NCAR 50-year reanalysis: monthly means CD-ROM and documentation. *Bull. Am. Meteorol. Soc.* 82, 247–268.
- Klein, S.A., Soden, B.J., Lau, N.-C., 1999. Remote sea surface temperature variations during ENSO: evidence for a tropical atmospheric bridge. *J. Climate*, 917–932.
- Kirtman, B.P., 1997. Oceanic Rossby wave dynamics and the ENSO period in a coupled model. *J. Climate* 10, 1690–1704.
- Large, W.G., McWilliams, J.C., Doney, S.C., 1994. Oceanic vertical mixing: a review and a model with a nonlocal boundary layer parameterization. *Rev. Geophys.* 32, 363–403.
- Landerer, F.W., Jungclaus, J.H., Marotzke, J., 2006. Regional dynamic and steric sea level change in response to the IPCC-A1B scenario. *J. Phys. Oceanogr.* 37, 296–312.
- Levitus, S., Antonov, J., Boyer, T., 2005. Warming of the world ocean, 1955–2003. *Geophys. Res. Lett.* 32, L02604.
- Li, L., Xu, J.D., Cai, R.S., 2002. Trends of sea level rise in the South China Sea during 1990s: an altimetry result. *Chin. Sci. Bull.* 47 (7), 582–585.
- Li, C., Mu, M., 1999. The occurrence of the El Niño event and the subsurface temperature anomaly of warm pool in the equatorial western Pacific. *Chin. J. Atmos. Sci.* 23, 513–526.
- Maes, C., 1998. Estimating the influence of salinity on sea level anomaly in the ocean. *Geophys. Res. Lett.* 25, 3551–3554.
- McPhaden, J., 1999. Genesis and evolution of the 1997–98 El Niño. *Science* 283, 950–954.
- Mellor, G.L., Yamada, T., 1982. Development of a turbulent closure model for geophysical and fluid problems. *Rev. Geophys.* 20, 851–875.
- Munk, W., 2002. Twentieth century sea level: an enigma. *Proc. Natl. Acad. Sci. USA* 99, 6550–6555.
- Philander, S.G.H., 1990. *El Niño, La Niña, and the Southern Oscillation*. Academic Press, San Diego, CA, 239pp.
- Qiu, D., Yang, T., Guo, Z., 1984. A westward current in the northeastern part of the South China Sea. *Trop. Oceanol.* 33, 65–73 (in Chinese with English abstract).
- Qu, T., Du, Y., Meyers, G., Ishida, A., Wang, D., 2005. Connecting the tropical Pacific with Indian Ocean through South China Sea. *Geophys. Res. Lett.* 32, L24609.
- Qu, K., Du, Y., Sasaki, H., 2006. South China Sea throughflow: a heat and fresh water conveyor. *Geophys. Res. Lett.* 33, L23617.
- Qu, K., Kim, Y.Y., Yaremchuk, M., Tozuka, T., Ishida, A., Yamagata, T., 2004. Can Luzon Strait transport play a role in conveying the impact of ENSO to the South China Sea? *J. Climate* 17, 3644–3657.
- Reynolds, R.W., Smith, T.M., 1994. Improved global sea surface temperature analyses using optimum interpolation. *J. Climate* 7, 929–948.
- Rong, Z., Liu, Y., Zong, H., Cheng, Y., 2007. Interannual sea level variability in the South China Sea and its response to ENSO. *Global Planet. Change* 55 (4), 257–272.
- Shaw, P.T., Chao, S.Y., Fu, L.L., 1999. Sea surface height variations in the South China Sea from satellite altimetry. *Oceanol. Acta* 22 (1), 1–17.
- Smith, W.H.F., Sandwell, D.T., 1997. Global seafloor topography from satellite altimetry and ship depth soundings. *Science* 277, 1956–1962.
- Tian, J., Yang, Q., Liang, X., Xie, L., Hu, D., Wang, F., Qu, T., 2006. Observation of Luzon Strait transport. *Geophys. Res. Lett.* 33, L19607.
- Trenberth, K.E., 1997. The definition of El Niño. *Bull. Am. Meteorol. Soc.* 78, 2771–2777.
- Wang, W., Wang, D., Qi, Y., 2000. Large-scale characteristics of interannual variability of sea surface temperature in the South China Sea. *Acta Oceanol. Sin.* 22, 8–16.
- Wang, W., Wang, C., 2006. Formation and decay of the spring warm pool in the South China Sea. *Geophys. Res. Lett.* 33, L02615.
- Wang, Y., Fang, G., Wei, Z., Qiao, F., Chen, H., 2006. Interannual variation of the South China Sea circulation and its relation to El Niño, as seen from a variable grid global ocean model. *J. Geophys. Res.* 111, C11S14.
- Willis, J.K., Roemmich, D., Cornuelle, B., 2004. Interannual variability in upper ocean heat content, temperature, and thermosteric expansion on global scales. *J. Geophys. Res.* 109, C12036.
- Xie, P., Arkin, P., 1997. A 17-year monthly climatology based on gauge observations, satellite estimates and numerical model outputs. *Bull. Am. Meteorol. Soc.* 78, 2539–2558.
- Xie, S.P., Xie, Q., Wang, D., Liu, W.T., 2003. Summer upwelling in the South China Sea and its role in regional climate variations. *J. Geophys. Res.* 108 (C8), 3261.
- Zebiak, S., 1989. Oceanic heat content variability and El Niño cycles. *J. Phys. Oceanogr.* 19, 475–486.
- Zhang, R.H., Levitus, S., 1997. Interannual variability of the coupled tropical Pacific Ocean-atmosphere system associated with the El Niño-Southern Oscillation. *J. Climate* 10, 1312–1330.
- Zheng, Z.W., Ho, C.R., Kuo, N.J., 2007. Mechanism of weakening of west Luzon eddy during La Niña years. *Geophys. Res. Lett.* 34, L11604.